Available online at www.sciencedirect.com

SciVerse ScienceDirect

Ceramics International 38 (2012) 1235–1240

CERAMICS INTERNATIONAL

www.elsevier.com/locate/ceramint

Nanograin Mn–Zn ferrite smart cores to miniaturize electronic devices

H. Waqas [a,*], A.H. Qureshi [a], K. Subhan [b], M. Shahzad [a]

[a] *Materials Division, PINSTECH, Islamabad, Pakistan*

[b] *Elecronic and Maintenance Division, PINSTECH, Islamabad, Pakistan*

Received 22 July 2011; received in revised form 24 August 2011; accepted 24 August 2011

Available online 2 September 2011

Abstract

Conventional ceramic and sol–gel auto combustion routes were adopted to develop Mn–Zn ferrite cores. To control high frequency (>500 kHz) losses, zirconia (0.2 wt%) and calcia (0.04 wt%) were added in $Mn_{0.57}Zn_{0.35}Fe_{2.08}O_4$. The results revealed that Mn–Zn ferrite smart cores synthesized by auto combustion process have superior properties than conventionally prepared cores. It is believed that the presence of unique properties such as nanograin microstructure, light weight and short height (thickness) dimensions have played their role to enhance the magnetic impedance of smart core to manifold. Fabricated smart core excellently performed in a test frequency band of 3–15 MHz.

Keywords: Mn–Zn ferrite; Auto combustion; Nanograin; Sintering; Gain; Impedance

1. Introduction

Mn–Zn ferrites (MZF) are famous for their extensive utilization in modern electronic devices such as switch mode power supplies, EMI suppression, data transmission circuitry, spintronic devices and also used as ferrofluids for biomedical applications [1–4]. MZF come under the umbrella of soft ferrites and chemically symbolized by MFe_2O_4. Where 'M' may be single or combination of divalent/multivalent metal ions (Fe^{2+}, Fe^{3+}, Mn^{2+}, Zn^{2+}, Zr^{4+}, Ti^{4+}, etc.) These ions are used to tailor the intrinsic properties of soft ferrites [5–7].

Ferrite cores are integral part of switch mode power supplies (SMPS). These are used to transmit the input power signals to other circuitry components without any loss. They also shield the electronic components against intense voltage surges. Up to 2 MHz frequency, Mn–Zn ferrite cores are efficiently working due to possessing high initial permeability with minimum core losses and commonly fabricated by conventional ceramic route [2,8]. But with the development of new technological and compact size devices, those are extensively used in our daily life such as high speed personal computers or laptops demanded the need of modified SMPS having minimum power dissipation. Similarly, telecommunication devices required SMPS which can be operated at higher frequencies without creating electromagnetic interferences [1]. In order to meet these requirements, there is need to fabricate ferrite cores having smaller dimensions and extended operational frequencies. The problem of power losses in MZF cores above 500 kHz is very common. It has been noted [9] that the initiation of ionic conduction (hopping mechanism) within/across the grains/grain boundaries generates eddy currents those restrict the functionality of Mn–Zn ferrite cores at higher frequencies. Many researchers [6,10,11] have tried to resolve this issue by dding/substituting different elemental oxides along with impurities in base compositions. It has been reported [10,12] that zirconia (ZrO_2) can be used to inhibit the grain growth process, while calcia (CaO) is famous to increase the grain boundary resistance of Mn–Zn ferrites. The optimum addition of these oxides may help to reduce the losses at higher frequencies. The alternate approach to tackle high frequency losses in Mn–Zn ferrites is the control of microstructure by exploiting nano science and technology. For this purposes, wet chemical routes such as sol gel [13], sol gel auto combustion [14], co-precipitation [15], hydrothermal [16] or mechano-synthesis processes [17] etc. have been employed to get nanosized powder of soft ferrites. It has been extensively reported [18–20] that smaller grains help to minimize power losses (eddy current) at higher frequencies. Sol–gel auto

* Corresponding author. Tel.: +92 512207226; fax: +92 512207374.
E-mail address: hw_pk@yahoo.com (H. Waqas).

0272-8842/$36.00
doi:10.1016/j.ceramint.2011.08.054

combustion process is one of the best synthesis techniques to produce nanosized powders of both metallic and non-metallic oxides. The compounds having complex structures like peroviskite (ferroelectric) and spinel (ferrite) have also been synthesized lucratively by this method. Sol–gel auto combustion method is very quick, simple and cheaper than other chemical processes. Because of its magnificent performance and high yield ratio, it is being commercialized to get nanosized powders for advanced ceramics industry [21].

Present research deals with comparative study of conventional ceramic and sol–gel auto combustion routes regarding synthesis and sintering of Mn–Zn ferrite cores (toroids). The synergistic effects of ZrO_2 and CaO on microstructure and electromagnetic properties such as magnetic impedance, resonance frequency and gain (G_{dB}) response [22] of newly developed Mn–Zn ferrite smart core have also been discussed.

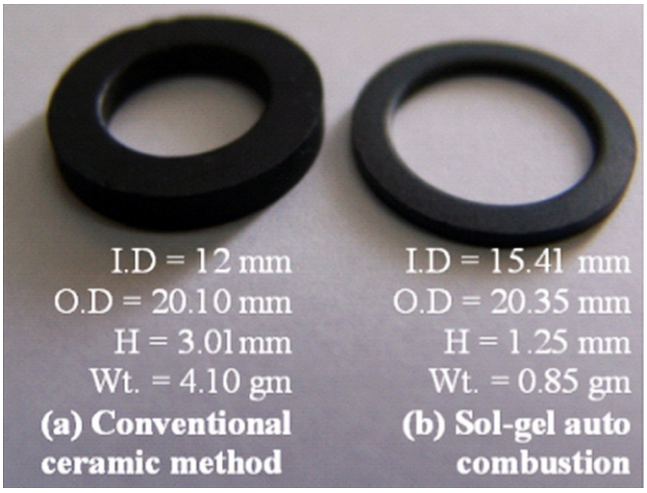

Fig. 1. Specifications of ZrO_2 and CaO added Mn–Zn Ferrite cores (toroid) fabricated by different processing routes.

2. Experimental procedure

Pure Mn–Zn ferrite ($Mn_{0.57}Zn_{0.35}Fe_{2.08}O_4$) and ZrO_2 (0.2 wt%) and CaO (0.04 wt%) added compositions were synthesized by conventional ceramic route using high purity (>99%) oxides of manganese, zinc, iron, zirconium and calcium oxides. Each composition was prepared by milling the required proportion of oxides for 8 h and calcination was done at 900 °C for 2 h in air. Calcined powders were again milled for 8 h to deagglomerate the powder particles and pressed under uniaxial load to obtain cores (toroids). The pressed cores of base composition (A1-O) and zirconia (ZrO_2) and calcia (CaO) added composition (A2-O) were sintered at 1350 °C for 2 h in controlled inert (N_2) atmosphere and cooled down to room temperature.

In sol–gel auto combustion process, nitrate solution of manganese, zinc, iron, zirconium and calcium was prepared in demineralized water (DMW). Citric acid and aqueous ammonia were added in an appropriate amount to adjust fuel to oxidant ratio as described elsewhere [14]. This solution was evaporated at 75 °C to get dry gel. The gel was ignited at 220 °C to obtain fine fluffy powder of Mn–Zn Ferrite containing 0.2 wt% zirconia (ZrO_2) and 0.04 wt% calcia (CaO). This powder was calcined in air at 450 °C for 30 min to remove un-burnt nitrate species. Green core (toroid) was obtained by uniaxial press (A3-G). Sintering was done at 1000 °C for 3 h in air and then 2 h further in N_2 at same temperature and cooled down to room temperature, according to sintering procedure explained by author elsewhere [23].

Dimensional comparison of sintered Mn–Zn ferrite cores for both processing routes can be viewed in Fig. 1. It can be observed that core produced by auto combustion process have more compact dimension than conventionally prepared core indicating its potential to miniaturize the electronic devices.

The X-ray diffraction (XRD) analysis of sintered cores was done by using diffractometer of Bruker (D-5005) having Cu K_α radiation source (k = 1.5406 Å). The data was collected in range from 20° to 70° with a scan rate of 0.02°/s. Sintered density was measured by Archimedes principal. Microstructure was determined by field emission electron microscope (Philip, XL-30). The magnetic impedance (mag-impedance) was measured by Agilent-4294A precision impedance analyzer with magnetic test fixture-16454A. Laboratory built circuit (Fig. 7a) was used to measure gain (G_{dB}) response of smart core (A3-G) as a function of high frequency signals i.e. 3–15 MHz.

3. Results and discussion

3.1. XRD analysis

The XRD patterns of sintered cores A1-O and A2-O synthesized by conventional ceramic route is shown in Fig. 2(a and b). These figures indicate well defined peaks of spinel phase that was developed during sintering. However, some peaks of nonmagnetic phase (Fe_3O_3) can also be observed in each diffraction pattern. The formation of small fraction of nonmagnetic phase was mainly due to the partial oxidation of Mn–Zn ferrite (spinel). During sintering, oxidation of conventionally prepared Mn–Zn ferrite is very common. There are many reasons for this problem, such as presence of impurities in metal oxide salts, high temperature kinetics those are involved to start solid state reactions among the ionic species. Moreover, the control of furnace environment during complete sintering cycle is also very crucial [23]. All these issues challenge the existence of single phase Mn–Zn ferrites processed through conventional ceramic route. Whereas, Fig. 2(c) represents XRD pattern of sintered core (A3-G) synthesized by sol–gel auto combustion route. Diffraction pattern shows the formation of single phase (spinel) Mn–Zn ferrites. No peak of nonmagnetic phase (Fe_2O_3) can be observed in this case. Synthesis of single phase (spinel) nanosized Mn–Zn ferrite powder is one of the distinctive features of auto combustion process. During its sintering at low temperature (1000 °C), emphasis was given to retain already developed spinel phase by controlling the oxidation/reduction reactions among nanosized Mn–Zn ferrite powder particles according to procedure as described by authors previously [23].

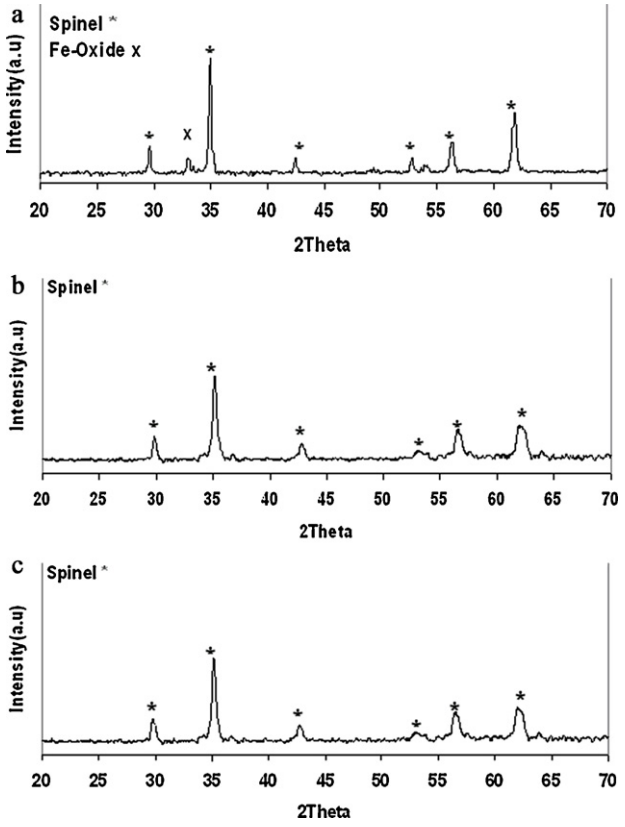

Fig. 2. (a) XRD pattern of Mn–Zn ferrite (A1-O) synthesized by conventional ceramic method and sintered at 1350 °C for 2 h. (b) XRD pattern of ZrO_2 and CaO added Mn–Zn ferrite (A2-O) synthesized by conventional ceramic method and sintered at 1350 °C for 2 h. (c) XRD pattern of ZrO_2 and CaO added Mn–Zn ferrite (A3-G) synthesized by sol–gel auto combustion method and sintered at 1000 °C.

3.2. Microstructure analysis

Fig. 3(a) represents the micrograph of sintered composition (A1-O). Which shows that microstructure is composed of larger and smaller grains. It is a true representation of abnormal grain growth (AGG) process [24]. This process mainly occurred in compounds having angular grain morphologies like ferrites, alumina, etc. Angular grains have singular interfaces possessing high interfacial energy as compared to spherical grains. This energy is named as two dimensions nucleation energy (2-DN) [25]. If the faces of adjacent grains have enough potential to overcome 2-DN barrier then interface will disappear and both of the neighboring grains will merge to form larger one. It is a random process, which may lead to abnormal grain growth (AAG) and ultimately produces irregular microstructure as it was observed in present situation. By employing linear intercept method, average grains size was calculated as 33 ± 5 μm and 97% of theoretical density (TD) was achieved after sintering. Large grain sizes although support the magnetic properties but on the other side these act as obstacle to meet high frequency requirements.

In order to refine the microstructure of Mn–Zn ferrite, ZrO_2 (0.2 wt%) and CaO (0.04 wt%) were simultaneously added (A2-O) and its micrograph after sintering is shown in Fig. 3(b). The micrograph clearly indicates that AGG effect has been remarkably suppressed with addition of zirconia and calcia. Average grain size of 21 μm (36% reduction in grain size) and 97.74% of the theoretical density was obtained with these additions. It has been reported [26] that zirconium is well known grain growth inhibitor. Grain growth inhibitors have very limited solubility in host lattice and usually reside at grain boundaries [27]. They fairly interact with grain boundaries and produce a drag force against their motion as a result inhibit the growth process. In present research, same phenomenon was observed with addition of zirconia (ZrO_2) in Mn–Zn ferrite and more homogenized microstructure (Fig. 3(b)) was obtained after sintering. Uniform/homogenize microstructure is highly desirable in Mn–Zn ferrites which helps to reduce high frequency losses. In order to investigate the dispersion of zirconia and calcia in Mn–Zn ferrite, EDS analysis of sintered sample (A2-O) was performed at different positions i.e. at the center of grain (position A) and along the grain boundaries (at positions B and C) as shown in Fig. 4. Elemental analysis (wt%/at%) at each position is given in Table 1. Table 1 shows that the concentrations of zirconia and calcia are higher at boundaries than the center of grain. This result verifies the above

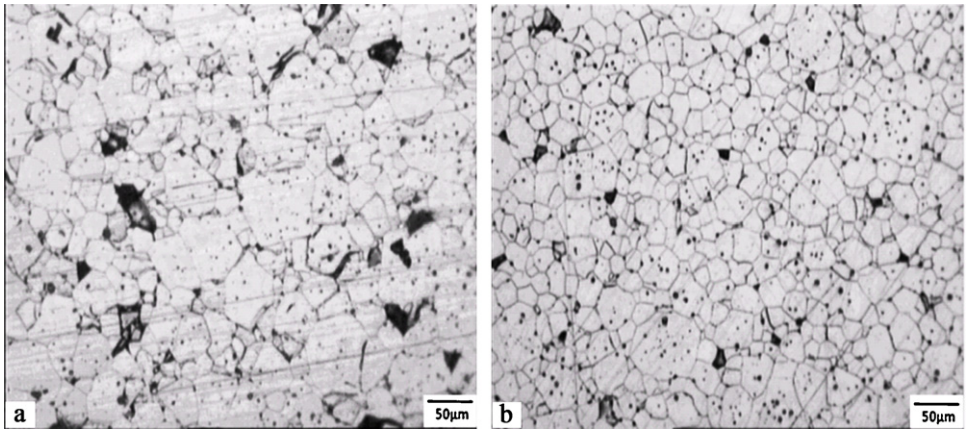

Fig. 3. (a and b) Microstructure of (a) pure Mn–Zn ferrite (b) ZrO_2 and CaO added Mn–Zn ferrite synthesized by conventional ceramic method and sintered at 1350 °C.

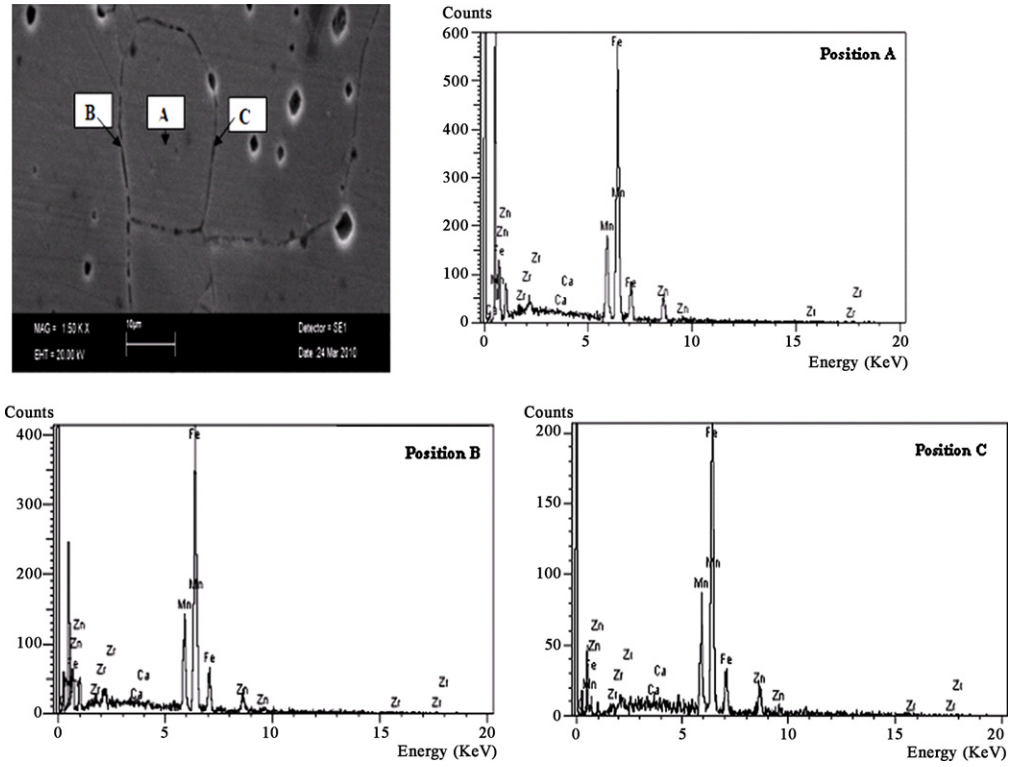

Fig. 4. EDS analysis of ZrO_2 and CaO added Mn–Zn ferrite (A2-O) synthesized by conventional ceramic method and sintered at 1350 °C.

mentioned statement i.e. grain growth inhibitors preferably reside at grain boundaries and help to reduce the grain sizes by immobilizing the grain boundaries.

The microstructure of composition (A3-G) synthesized by sol–gel auto combustion process and sintered at 1000 °C for 5 h under controlled atmospheric (N_2) conditions is shown in Fig. 5. The average grain size was calculated as 0.15 ± 0.01 μm and 91% of theoretical density was obtained after sintering. This result shows that 99.28% of grain size has been reduced by employing sol–gel auto combustion route. Nanosized synthesis of Mn–Zn ferrite powder and low sintering temperature are the main factors to modify the microstructure of Mn–Zn ferrites as discussed by authors elsewhere [14,23].

3.3. Magnetic impedance

Fig. 6 shows mag-impedance curves of sintered Mn–Zn ferrite cores (A1-O, A2-O, A3-G). It can be observed that A1-O has maximum impedance of 50 Ω with resonance frequency (f_r) of 58 MHz. With the addition of zirconia and calcia the impedance resistance has been increased to 70 Ω while no significant effect was observed for resonance frequency. These results indicate that the presence of zirconia has increased electrical resistance by reducing grain size and introducing more grain boundaries within the microstructure. Furthermore, it has been reported by many researchers [6,28–30] that calcium oxide preferred to segregate along grain boundaries rather to dissolve in spinel lattice the same effect of calcia was observed in present case (Fig. 4). Calcia

Table 1
EDS analysis of composition (A2-O) at A (center of grain), B (grain boundary) and C (grain boundary) positions.

Element type	Job: demonstration data SiLi detector System resolution = 62 eV Quantitative method: ZAF (2 iterations).			Standards: Ca K Wollas 23/11/93 Mn K Mn 01/12/93Fe K Fe 01/12/93 Zn K Zn 01/12/93 Zr L Zr 01/12/93		
	wt%			at%		
	A	B	C	A	B	C
Fe K	64.69	62.38	67.58	66.35	64.08	68.79
Mn K	16.41	17.19	18.93	17.11	17.95	19.58
Zn K	18.56	19.29	12.93	16.26	16.93	11.24
Zr L	0.26	0.72	0.53	0.16	0.45	0.33
Ca K	0.08	0.42	0.04	0.12	0.60	0.06

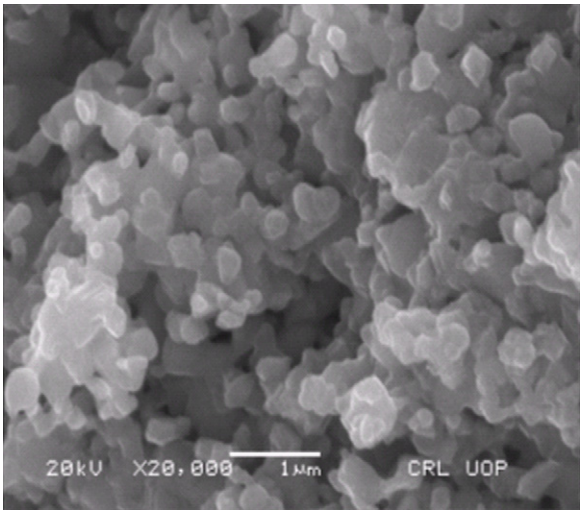

Fig. 5. Microstructure of ZrO_2 and CaO added Mn–Zn ferrite (A3-G) synthesized by sol–gel auto combustion method and sintered at 1000 °C.

reacted with un-dissolved zirconia and made some secondary phases (Ca–ZrO_2) along the boundaries which had further enhanced the impedance resistance of Mn–Zn ferrites. The composition (A3-G) has highest magnetic impedance (395 Ω) and resonance frequency (64 MHz) as shown in Fig. 6. These highest values are due to the development of homogenized microstructure that was achieved through auto combustion route. The presence of nano-grains extensively increased the volume fraction of grain boundaries in microstructure as a result further enhancement in the impedance resistance [31] of zirconia and calcia added composition was observed. These smaller size grains have also the ability to vibrate at high frequency signals and help to increase the resonance frequency of Mn–Zn ferrites.

3.4. Frequency gain response

In order to verify the performance of fabricated smart core (A3-G) by auto combustion process, gain (G_{dB}) values were

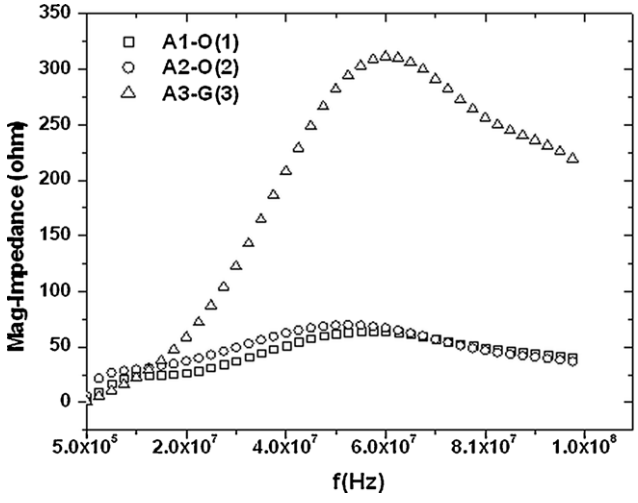

Fig. 6. Magnetic impedance (mag-impedance) of A1-O, A2-O and A3-G compositions.

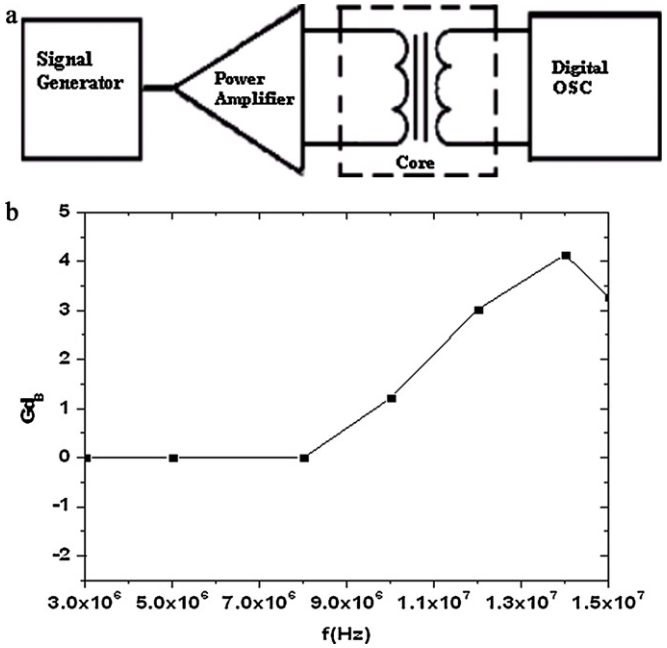

Fig. 7. (a and b) Gain (G_{dB}) measurement of smart Mn–Zn ferrite core (a) Laboratory built circuit (b) Gain (G_{dB}) response curve of Mn–Zn ferrite smart core (A3-G).

determined by using the laboratory built circuit (Fig. 7(a)) for high frequency range of 3–15 MHz as shown in Fig. 7(b). This figure indicates that core has positive G_{dB} values within the selected frequency range. A sharp increase in gain can be observed after 8 MHz which might be due to the resonance effect coming from other circuitry components. However, no negative G_{dB} values was observed during this analysis which indicated that all the input signals supplied to core through primary circuit have been transferred to secondary side without any loss. In fact the presence of nanograins have enabled the smart core (A3-G) to well respond against high frequency signals and due to possessing high impedance resistance, leakage current within or across the grains has been remarkably suppressed as result high frequency response in smart core was observed. It is believed that this newly developed Mn–Zn ferrite smart core have an ability to overcome transmission losses during its operation.

4. Conclusion

From above discussion, it can be concluded that Mn–Zn ferrite containing zirconia (ZrO_2) and calcia (CaO) is one of the best compositions suitable for high frequency applications due to possessing high mag-impedance and resonance frequency. Furthermore, the choice of appropriate processing route like sol–gel auto combustion method further enhances the mag-impedance of Mn–Zn ferrites to manifolds as compared to conventional ceramic method due to the advantage of nanograins microstructure, low sintering temperature and ability to fabricate light weight and compact size cores.

Acknowledgements

Authors would like to thank central diagnostic Lab. PINSTECH and central research Lab. University of Peshawar for providing characterization facilities.

References

[1] K. Yanagisawa, F. Zhang, T. Sato, K. Yamasawa, Y. Miura, A new wideband common-mode noise filter consisting of Mn–Zn ferrite core and copper/polyimide tape wound coil, IEEE Trans. Magn. 41 (2005) 3571–3573.
[2] A.H. Qureshi, The Influence of hafnia and impurities (CaO/SiO_2) on the microstructure and magnetic properties of Mn–Zn ferrites, J. Cryst. Growth 286 (2006) 365–370.
[3] M.S. Tomar, S.P. Singh, O.P. Perez, R.P. Guzman, E. Calderon, C.R. Ramos, Synthesis and magnetic behavior of nanostructured ferrites for spintronics, Microelectron. J. 36 (2005) 475–479.
[4] R. Arulmurugana, G. Vaidyanathana, S. Sendhilnathanb, B. Jeyadevan, Mn–Zn ferrite nanoparticles for ferrofluid preparation: study on thermal–magnetic properties, J. Magn. Magn. Mater. 298 (2006) 83–94.
[5] E. Kester, B. Gillot, C. Villette, P. Tailhades, A. Rousset, Valence states of copper in copper ferrite spinels $Cu_xFe_{3-x}O_4$ ($0 < x \leq 1$) fine powders: evidence of copper insertion, Thermoacetica Acta 297 (1997) 71–77.
[6] H. Shokrollahi, K. Janghorban, Influence of additives on the magnetic properties, microstructure and densification of Mn–Zn soft ferrites, Mater. Sci. Eng. B 141 (2007) 91–107.
[7] M.M. Hessien, M.M. Rashad, K. El-Barawy, I.A. Ibrahim, Distortions of the statistical distribution of barkhausen noise measured by magneto-optical kerr effect, J. Magn. Magn. Mater. 320 (2008) 1651–1656.
[8] J. Fan, F.R. Sale, Analysis of power loss on Mn–Zn ferrites prepared by different processing route, IEEE Trans. Magn. 32 (1996) 4854–4856.
[9] C. Beatrice, F. Fiorillo, Measurement and prediction of magnetic losses in Mn–Zn ferrites from dc to the megahertz range, IEEE Trans. Magn. 42 (2006) 2867–2869.
[10] W.H. Jeong, B.M. Song, Y.H. Han, Analysis of power losses in Mn–Zn ferrites, Jpn. J. Appl. Phys. 41 (2002) 2912–2915.
[11] H. Shokrollahi, Magnetic properties and densification of manganese–zinc soft ferrites ($Mn_{1-x}Zn_xFe_2O_4$) doped with low melting point oxides, J. Magn. Magn. Mater. 320 (2008) 463–474.
[12] J. Fan, N. Foong-Kee, R.F. Sale, Magnetic properties and microstructures of SnO_2 doped Mn–Zn ferrites, Rare Met. 25 (2006) 445–449.
[13] A. Thakur, M. Singh, Preparation and characterization of nanosize $Mn_{0.4}Zn_{0.6}Fe_2O_4$ ferrite by citrate precursor method, Ceram. Int. 29 (2003) 505–511.
[14] H. Waqas, A.H. Qureshi, Influence of pH on nanosized Mn–Zn ferrite synthesized by sol–gel auto combustion process, J. Therm. Anal. Calorim. 98 (2009) 355–360.
[15] B. Jeyadevan, K. Tohji, K. Nakatsuka, A. Narayanasamy, Irregular distribution of metal ions in ferrites prepared by co-precipitation technique structure analysis of Mn–Zn Ferrite using extended X-ray absorption fine structure, J. Magn. Magn. Mater. 217 (2000) 99–105.
[16] Y. Xuan, Q. Li, G. Yang, Synthesis and magnetic properties of Mn–Zn ferrite nanoparticles, J. Magn. Magn. Mater. 312 (2007) 464–469.
[17] N. Guigue-Millot, S. Begin-Colin, Y. Champion, M.J.H. ytch, G. Le, Ca. er, P. Perriat, Control of grain size and morphologies of nanograined ferrites by adaptation of the synthesis route: mechanosynthesis and soft chemistry, J. Solid State Chem. 170 (2003) 30–38.
[18] W.H. Jeong, Y.H. Han, Effects of grain size on the residual loss of Mn–Zn ferrites, J. Appl. Phys. 91 (2002) 7619–7621.
[19] M.T. Johnson, E.G. Visser, A coherent model for the complex permeability in polycrystalline ferrites, IEEE Trans. Magn. 26 (1990) 1987–1989.
[20] Y. Yamamoto, A. Makino, Core losses and magnetic properties of Mn–Zn ferrites with fine grain sizes, J. Magn. Magn. Mater. 133 (1994) 500–503.
[21] S.T. Aruna, S. Alexander, Mukasyan, Combustion synthesis and nano-mateials, Curr. Opin. Solid State Mater. 12 (2008) 44–50.
[22] O. Dezuari, S.E. Gilbert, E. Belloy, M.A.M. Gijs, High Inductance planar transformers, Sens. Actuators 81 (2000) 355–358.
[23] H. Waqas, A.H. Qureshi, Low temperature sintering study of nanosized Mn–Zn ferrites synthesized by sol–gel auto combustion process, J. Therm. Anal. Calorim. 100 (2010) 529–535.
[24] G. Jeong, J. Choi, S. Kim, Abnormal grain growth and magnetic loss in Mn–Zn ferrites containing CaO and SiO_2, IEEE Trans. Magn. 36 (2000) 3405–3407.
[25] Y.J. Park, N.M. Hwang, D.N. Yoon, Abnormal growth of faceted (WC) grains in a (Co) liquid matrix, Metall. Mater. Trans. A 27 (1996) 2809–2819.
[26] T. Otsuki, E. Otsuki, T. Sato, K. Shoji, Effect of additive on magnetic properties and microstructure of Mn–Zn ferrites for high-frequency power supply, in: Proceedings of 6th International Conference on Ferrites (ICF-6), Tokyo, Japan, September 29–October 2, 1992.
[27] M. Daniil, Y. Zhang, H. Okumura, G.C. Hadjipanayis, D.J. Sellmyer, Effect of grain growth inhibitors on the hysteresis properties of $Nd_{10}Fe_{82}C_6B_2$ melt-spun alloys, IEEE Trans. Magn. 38 (2002) 2973–2975.
[28] J. Laval, C. Cabanel, M. Berger, Local electrical behaviour, crystallography and chemistry of grain boundaries in Mn–Zn ferrites, J. Am. Ceram. Soc. 81 (1998) 1133–1140.
[29] S. Otobe, Y. Yachi, T. Hashimoto, T. Shigenage, H. Takei, K. Hontani, Development of low loss Mn–Zn ferrites having the fine microstructure, IEEE Trans. Magn. 35 (1999) 3409–3411.
[30] J.S. Lee, Misorientation distribution of a Mn–Zn ferrite sample with abnormal grain growth, J. Ceram. Process. Res. 5 (2004) 179–186.
[31] K.M. Batoo, S. Kumar, C.G. Lee, Alimuddin, study of ac impedance spectroscopy of Al doped $MnFe_{2-2x}Al_{2x}O_4$, J. Alloys Compd. 480 (2009) 596–602.